Available online at www.sciencedirect.com
SCIENCE DIRECT®
Journal of Chromatography A, 1083 (2005) 68–79
JOURNAL OF CHROMATOGRAPHY A
www.elsevier.com/locate/chroma

Stress distribution and dimensional changes in chromatographic columns

Feng Chen [a], Eric. C. Drumm [a], Georges Guiochon [b,c,*]

[a] *Department of Civil and Environmental Engineering, University of Tennessee, Knoxville, TN 37996-2010, USA*
[b] *Department of Chemistry, University of Tennessee, Knoxville, TN 37996-1600, USA*
[c] *Division of Chemical Sciences, Oak Ridge National Laboratory, Oak Ridge, TN 37831-6120, USA*

Received 3 May 2005; accepted 1 June 2005

Abstract

High pressures, in the kilobar range, are now used in liquid chromatography. Basic equations from mechanics are applied to investigate the stress state in several idealized chromatography tubes, and these stresses are evaluated with respect to the maximum allowable stresses predicted by several methods used in pressure vessel design. An analytical solution is developed for the dimensional changes of idealized tubes subjected to internal pressure, and the analytical solutions used to verify the results from a numerical approximation. Numerical approximations are then used to explore the effects of the end restraint provided by the end frits. Conclusions are derived regarding the requirements for a safe operation of these high pressure chromatography tubes.

Keywords: Chromatography tube; High pressure; Dimensional change; Factor of safety

1. Introduction

For a variety of reasons that were discussed earlier [1,2], a new trend is gaining strength in liquid chromatography. Analysts are beginning to use columns packed with small particles, with diameters in the 1–2 μm range, that are operated at high mobile phase velocities, and that can generate high efficiencies in short analysis times [3,4]. These high performance can be achieved only if a high inlet pressure, of the order of 1–1.5 kbar, is applied. Further gains, currently actively contemplated, would require the use of still higher inlet pressures, in the range of several kbar. Therefore, it is useful at this stage to evaluate the resulting stresses in the column tube compared to the yield or limit stresses of typical tube materials. It is also in interest to determine the effects of these high pressures on the actual dimensional changes of the column tube. The first question has implications regarding appropriate pressure levels for the safe use of such columns, while the latter questions may have implications relative to changes in the column porosity due to volume changes during operation, hence to the prediction of column performance when the flow rate is adjusted. This work answers these questions. The notation used in the development of the expressions for the stress and the deformation of column tubes is provided in Table 1.

The problem consists of determining the stresses and strains in the tube used to pack a chromatographic column. Table 2 lists typical dimensions for several models of such columns made from stainless steel and silica while Table 3 lists some typical mechanical properties for these materials. A schematic of a tube is shown in Fig. 1, where the ends of the tube are closed with frits. If the tube is very long with respect to the diameter, and it is assumed to behave in a linear elastic manner, the principle of superposition is valid. Thus, the radial deformations due to the pressure acting on the tube wall can be investigated independently from the axial deformations due to the pressure acting on the tube ends, and

* Corresponding author. Tel.: +1 865 974 0733; fax: +1 865 974 2667.
E-mail address: guiochon@utk.edu (G. Guiochon).

0021-9673/$ – see front matter © 2005 Published by Elsevier B.V.
doi:10.1016/j.chroma.2005.06.004

Table 1
Table of notation

L_0	Original tube length
ΔL	Change in tube length
L	Tube length after deformation
Δr	Change in radius
r	Distance from the z-axis in the $r-\theta$ plane
$r_{in,0}$	Original internal radius
r_{in}	External radius after deformation
$r_{ext,0}$	Original external radius
r_{ext}	External radius after deformation
r_m	Average radius
t	Tube thickness
P_{max}	Maximum pressure at the column inlet
p_s	Internal equivalent uniform pressure
μ	Poisson's ratio
E	Young's modulus
σ_r	Radial stress
σ_θ	Circumferential stress
σ_z	Vertical stress
σ_1, σ_2, σ_3	Principle stresses
σ_m	Mean stress
σ_s	Deviator stress
σ_{avg}	Average stress along the tube wall (membrane stress)
$\sigma_{y.p.}$	Material yield stress
σ_{ult}	Material ultimate stress
σ_{max}	Maximum stress
τ_{max}	Maximum shear stress
U	Total strain energy produced in an element
U_v	Energy of volume change per unit of volume
U_d	Energy of distortion per unit of volume
$U_{d,tension}$	Energy of distortion per unit of volume under simple tension case
K_p	Stiffness of the end frit
K_t	Stiffness of the tube

the results superimposed. These two effects are depicted in Fig. 2, where a uniform pressure throughout the tube has been assumed. The stresses induced in a pressurized tube will be described. The stresses developed in typical chromatographic columns are different since the column is not subject to a uniform internal pressure, as a pressurized closed vessel, but to a pressure gradient that can be considered as a first approximation as linear. These stresses will be compared with the limit stresses or yield stresses. The deformations of the tube will then be discussed.

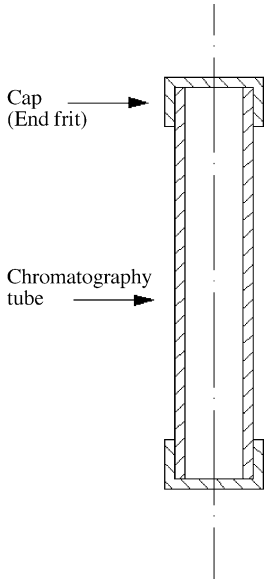

Fig. 1. Schematic of chromatography tube.

It is usually assumed that stainless steel has equal yield strength in tension and compression. Fused silica, on the other hand, has a tensile strength that is significantly less than its compressive strength. Exposed to air, a silica tube would rapidly lose its strength and become most brittle. Fused silica tubes used as chromatographic columns fabricated are sheathed with a layer of a cross-linked polymer that prevents its weathering under the influence of atmospheric water and ensures a long-term stability of the tensile strength of the material.

Table 2
Typical tube geometries

Tube	p_s (MPa)	Length, L (mm)	Internal radius, r_i (mm)	External radius, r_e (mm)	Mean radius, r_m (mm)	Thickness, t (mm)	r_m/t
SS-1	100	100	0.50	1.00	0.75	0.50	1.5
SS-2	100	100	2.30	3.15	2.73	0.85	3.2
SS-3	100	100	0.50	1.05	0.78	0.55	1.4
SS-4	100	100	2.69	3.18	2.93	0.48	6.1
SC-1	450	500	0.02	0.18	0.10	0.17	0.6
SC-2	680	500	0.05	0.18	0.12	0.13	0.9

Table 3
Table of assumed tube material properties

Tube	Materials	Elastic modulus (GPa)	Poisson's ratio (μ)	Tensile strength (MPa)	Compressive strength (MPa)
SS-1,2,3,4	Stainless steel	210 [8]	0.33	942	942
SC-1,2	Silica	73	0.17	4826 (689)[a]	N/A

[a] Based on the Si—O bond strength, the fiber has a theoretical tensile strength of ~2000 kpsi. In practice the observed tensile strength is considerably lower, typically 700 kpsi (4826 MPa), due to the presence of small flaws in the bulk and on the surface of the silica [10], when in practical use, the tubes are generally 100% proof tested at 100 kpsi (689 MPa) [11].

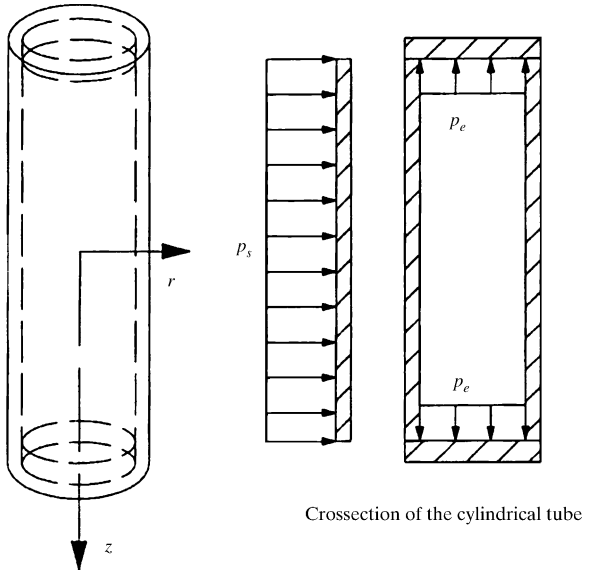

Fig. 2. Axis-symmetric model for the tube with wall and end pressures.

2. Theory

2.1. Analytical solution for the stresses in a pressured tube

If the tube is long relative to its diameter, and the pressure is assumed to be constant along the length of the tube, it can be assumed that the response of every section along the length is the same, and that all deformations act in a plane normal to the axis of the tube. This is referred to as the plane strain condition, and the stress components in this $r-\theta$ plane are shown in Fig. 3, where the $r-\theta$ plane is normal to the z-axis of the tube.

2.1.1. Stresses in the $r-\theta$ plane

From theory of elasticity, the cylinder subjected to an internal pressure p_s, Fig. 3, results in the following components of stress:

$$\sigma_r = \frac{r_i^2 p_s}{r_e^2 - r_i^2}\left(1 - \frac{r_e^2}{r^2}\right) \tag{1a}$$

$$\sigma_\theta = \frac{r_i^2 p_s}{r_e^2 - r_i^2}\left(1 + \frac{r_e^2}{r^2}\right) \tag{1b}$$

where σ_r, σ_θ are the radial and tangential stress at distance r from the axis z; σ_z is the stress component in the axial or z-direction and r_i, r_e are the initial internal and external radii.

The stress distribution in the z-direction is relatively simple. Suppose the pressure acting on the internal surface of the end frit is p_s, the resulting stress along the z-direction is uniform at any point in the $r-\theta$ plane:

$$\sigma_z = \frac{r_i^2 p_s}{r_e^2 - r_i^2} \tag{1c}$$

As suggested by Timoshenko and Goodier [5], the radial stress σ_r is always compressive and σ_θ, sometimes referred to as the hoop stress or circumferential stress, is tensile. The hoop stress σ_θ is greatest at the inner surface of the cylinder, where

$$\sigma_\theta = \sigma_{\theta\,\max} = \frac{(r_e^2 + r_i^2)p_s}{(r_e^2 - r_i^2)} \tag{2}$$

This maximum value $\sigma_{\theta\,\max}$ is always numerically greater than the internal pressure p_s but should diminish towards p_s as r_e increases. Regardless of the thickness of the tube, $\sigma_{\theta\,\max}$ can never be less than p_s, and σ_θ is the critical stress to investigate in a pressurized tube.

The three stress components at the inner surface of the column (radius $r_{in,0}$) are principal stresses:

$$\sigma_1 = \sigma_\theta = \frac{r_i^2 p_s}{r_e^2 - r_i^2} + \frac{r_e^2 p_s}{r_e^2 - r_i^2} = \sigma_m + \sigma_s \tag{3a}$$

$$\sigma_2 = \sigma_z = \frac{r_i^2 p_s}{r_e^2 - r_i^2} = \sigma_m \tag{3b}$$

$$\sigma_3 = \sigma_r = \frac{r_i^2 p_s}{r_e^2 - r_i^2} - \frac{r_e^2 p_s}{r_e^2 - r_i^2} = \sigma_m - \sigma_s \tag{3c}$$

where σ_1, σ_2, σ_3 are the major, the intermediate, and the minor principal stresses, respectively, σ_m the mean stress and σ_d is the deviator stress. The mean stress and the deviator stresses can be re-written as:

$$\sigma_m = \frac{r_i^2 p_s}{r_e^2 - r_i^2} \tag{4a}$$

$$\sigma_s = \frac{r_e^2 p_s}{r_e^2 - r_i^2} \tag{4b}$$

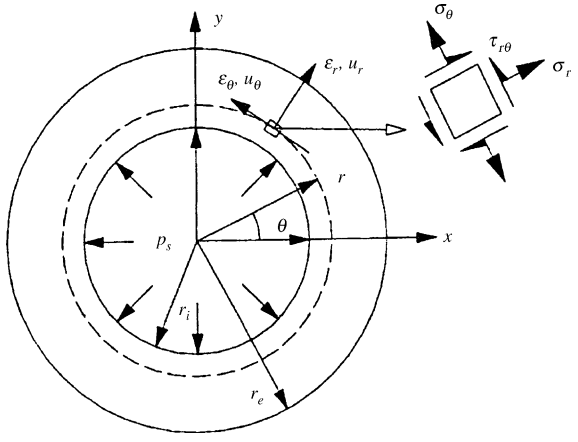

Fig. 3. Stress components on cross-section of the tube ($r-\theta$ plane).

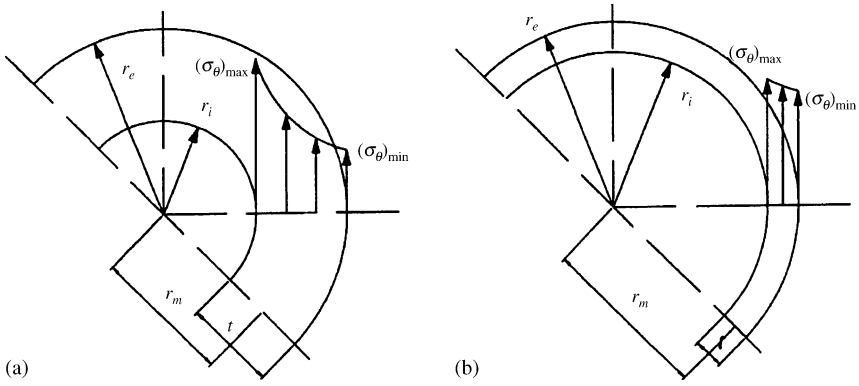

Fig. 4. Circumferential stress σ_θ in thick- and thin-walled tubes.

2.1.2. Stress distributions in thick-walled and thin-walled tubes

The distributions of the circumferential stress (σ_θ) across the wall of a thick- and thin-walled tubes are depicted in Fig. 4. Because the inside and outside radii of the thin-walled tube are nearly the same (Fig. 4b), the difference in the stresses at the inside and outside radii are not as great as that for a thick-walled tube (Fig. 4a). In the notation used for pressure vessel analysis, the circumferential stress in a thin-walled tube is often taken as the average of the inside and outside values of σ_θ, and is referred to as the membrane stress.

Thus, the circumferential stress in the thin-walled tube can be calculated by average stress as:

$$\sigma_{avg} = \frac{p_s r_m}{t} \tag{5}$$

where $r_m = (r_e + r_i)/2$ is the average radius of the tube, and t is the thickness of the tube wall. Although there is no universally accepted division between thin- and thick-walled vessels, the ASME pressure vessel code suggests that tubes with $r_m/t \geq 10$ can be treated as thin-walled tubes [6]. As indicated in Table 2, the typical chromatography tubes considered here do not meet this criteria, since r_m/t is less than 10. Therefore, these typical tubes would be considered to be thick-walled, where the maximum stress occurs at the inside radius and diminishes across the thickness, as shown in Fig. 4a. The following discussion of chromatographic column tube failure will be based on the thick-walled tube assumption.

2.2. Failure theories for pressured tubes

The strength of most materials, particularly metals, is typically determined in a simple uniaxial tension test, where the strength is often defined as the yield stress, $\sigma_{y.p.}$ at which the deformations are no longer recoverable, or alternately in terms of the ultimate stress σ_{ult}, which is the stress corresponding to the ultimate strength. When tubes or pressure vessels are designed for some internal pressure, the resulting stress state is compared with stress at failure, which is usually expressed as some fraction of the yield stress. In order to determine the allowable design stress for multi-axial stress conditions, several theories of failure have been developed. Their purpose is to estimate when failure will occur under the action of combined stresses on the basis of data obtained from simple tension or compression tests. Failure of the tube refers to either yielding or actual rupture of the material, whichever occurs first.

There are numerous theories to predict the state of stress at failure or the limit stress, among which three theories that are most commonly used in pressure vessel design to assure that the operating pressures are safe with respect to the anticipated stresses at failure. These theories consider both the combined state of stress and the uniaxial stress state. In this section, the application of these theories to investigate the service pressures in chromatography tubes will be discussed.

Even though the pressures in these tubes are high, it will be shown subsequently that the dimensional changes are small and as such, that the energy release upon failure would be small and the consequences of failure be minimal (besides the loss of the experimental data involved).

2.2.1. "Maximum stress" or Rankine theory

According to this theory, the failure of the tube is assumed to occur when the maximum principal stress reaches the yield stress in simple tension, $\sigma_1 = \sigma_{y.p.}$ As discussed above, for typical chromatographic columns, the maximum stress should be calculated as in a thick-walled tube according to Eq. (3a). Thus, for a given internal pressure, the following inequality should be maintained:

$$\sigma_{max} = \sigma_1 = \sigma_m + \sigma_s = \frac{r_i^2 p_s}{r_e^2 - r_i^2} + \frac{r_e^2 p_s}{r_e^2 - r_i^2} \leq \sigma_{y.p.} \tag{6a}$$

and the maximum internal pressure inside the tube is:

$$p_{s\_Rankine} \leq \frac{\sigma_{y.p.}(r_e^2 - r_i^2)}{r_e^2 + r_i^2} \tag{6b}$$

The maximum stress theory is often appropriate for materials that fail in a brittle manner, or those for which the strength in tension and compression are vastly different [7].

This may be the case for chromatographic tubes made of silica, which may fail in a brittle manner and has different yield strengths in compression and tension (Table 3).

2.2.2. "Maximum shear stress" or Tresca theory

This theory postulates that yielding in a body subject to combined stresses will occur when the maximum shear stress becomes equal to the maximum shear stress at yield in a simple tension test, which is the yield stress $\sigma_{y.p.}$. The maximum shear stress in the tube is equal to one-half the difference of the maximum and the minimum principal stress; thus, the maximum shear stress in the chromatographic tube is:

$$\tau_{max} = \frac{\sigma_1 - \sigma_3}{2} = \frac{\sigma_\theta - \sigma_r}{2} = \frac{r_e^2 p_s}{r_e^2 - r_i^2} \leq \frac{\sigma_{y.p.}}{2} \tag{7a}$$

and the corresponding maximum internal pressure inside the tube is:

$$p_{s\_Tresca} \leq \frac{\sigma_{y.p.}(r_e^2 - r_i^2)}{2r_e^2} \tag{7b}$$

For ductile materials such as steel, aluminum, and brass, and those materials for which the tensile and compressive strength are the same, the maximum shear stress theory may give better agreement with experimental results than the "maximum stress" theory [6–8]. Thus, this might be an appropriate theory for stainless steel chromatographic tubes (Table 3).

2.2.3. "Maximum distortion energy" or von Mises-Hencky theory

The maximum distortion energy, also known as the maximum octahedral shear stress theory, provides somewhat more accurate results that the maximum shear stress theory [7]. This theory assumes that the total strain can be resolved into two parts:

- The strain energy due to deformation in uniform tension or compression.
- The strain energy due to distortion or change in shape of the unit volume.

This can be written as:

$$U = U_v + U_d \tag{8}$$

where U_v is the energy of volume change per unit of volume, and U_d is the energy of distortion per unit of volume. It is further assumed that failure can be attributed only to the distortion strain energy. The calculation of U_d is:

$$U_d = \frac{1+\mu}{6E}[(\sigma_1 - \sigma_2)^2 + (\sigma_2 - \sigma_3)^2 + (\sigma_3 - \sigma_1)^2] \tag{9}$$

According to this theory, yielding begins when the distortion energy reaches the value of the distortion energy at the yield point in a simple tension test. In a simple tension-test, the yield point is obtained by substituting $\sigma_1 = \sigma_{y.p.}$, and $\sigma_2 = \sigma_3 = 0$ in Eq. (9) which gives

$$U_{d,tension} = \frac{1+\mu}{3E}\sigma_{y.p.}^2 \tag{10}$$

This theory has been widely used in pressure vessel design to assure that the inner bore of the vessel remains elastic, or below yield. In practice, the distortion energy stress is calculated and compared to the yield strength of the tube material. For the chromatography tube, substitution of Eq. (3) into the above Eq. (9) yields:

$$U_d = \frac{1+\mu}{6E}[\sigma_s^2 + \sigma_s^2 + (2\sigma_s)^2] = \frac{1+\mu}{E}\sigma_s^2 \tag{11}$$

To limit the distortion energy in Eq. (11) to values less than the yield stress in simple tension, given in Eq. (10), we must have $U_d < U_{d,tension}$, or:

$$\sigma_s = \frac{p_s r_i^2}{r_e^2 - r_i^2} \leq \frac{\sigma_{y.p.}}{\sqrt{3}} \tag{12a}$$

The corresponding maximum pressure in the tube is:

$$p_{s\_von\,Mises} \leq \frac{\sigma_{y.p.}(r_e^2 - r_i^2)}{\sqrt[3]{r_i^2}} \tag{12b}$$

2.2.4. Application of the failure theory to the tubes of chromatographic columns

For the design of pressurized tubes and vessels, the dimensions are selected such that the relevant stress in the vessel is below the stress at yield by a specified margin of safety, which is commonly presented as a factor of safety:

$$FS = \frac{\text{stress or pressure at failure}}{\text{stress or pressure under service}} > 1.0 \tag{13}$$

Typically, larger factors of safety are utilized to reflect a greater uncertainty in the service pressure, the material properties, the theory of failure or in cases when the consequence of failure is significant. Table 4 summarizes the three yield theories presented above, references the applicable section in the ASTM pressure vessel code with the recommended factor of safety [7]. Table 4 also indicates the expression for the maximum internal pressure as a function of yield stress and tube geometry. Note that as the complexity and reliability of the failure theory increases (Rankine theory versus Tresca theory versus von Mises theory), the recommended factor of safety decreases.

2.3. Analytical solution for radial and axial deformations

An analytical solution for the dimensional changes in a chromatography column was derived earlier, based on the assumption of linear elasticity, and the assumption that the tube is long with respect to the diameter such that the effects of the ends are negligible on the deformations [1]. The solution

Table 4
Summary of failure theories and maximum internal pressure

Basis		Maximum internal pressure, $p_{s,max}$	Equation	ASME code section	Factor of safety
Theory of failure	Material property				
Maximum stress or Rankine theory	Maximum stress in wall thickness reaches material tensile strength	$\frac{r_e^2-r_i^2}{r_e^2+r_i^2}\sigma_{y.p.}$	(6)	Section VIII-1 pressure vessels	4
Maximum shear stress or Tresca theory	Average shear stress in wall thickness reaches material ultimate shear stress	$\frac{r_e^2-r_i^2}{r_e^2}\frac{\sigma_{y.p.}}{2}$	(7)	Section VIII-2 Pressure Vessels	3
Distortion energy or von Mises-Hencky theory	Material yield strength first reached throughout wall thickness	$\frac{r_e^2-r_i^2}{r_e^2}\frac{\sigma_{y.p.}}{\sqrt{3}}$	(12)	Section VIII-3 pressure vessels	1.5

assumes the superimposition of the axial and radial deformations due to the internal pressure as depicted in Fig. 5. The assumed boundary conditions lead to a simple 2D model for the free end tube shown in Fig. 6. Because changes in the tube density due to the pressure can be neglected, and an axial (or a radial) expansion is accompanied by a radial (or an axial) constriction, the relative dimensional changes were obtained as [2]:

$$\frac{L}{L_0} = 1 + \frac{\Delta L}{L_0} = 1 + \frac{(1-2\mu)r_{in,0}^2}{r_{ext,0}^2 - r_{in,0}^2}\frac{p_s}{E} \tag{14a}$$

$$\frac{r_{in}}{r_{in,0}} = 1 + \frac{\Delta r_{in}}{r_{in,0}} = 1 + \frac{[(1+\mu)r_{in,0}^2 + (1-\mu)r_{in,0}^2]}{r_{ext,0}^2 - r_{in,0}^2}\frac{p_s}{E} \tag{14b}$$

$$\frac{r_{ext}}{r_{ext,0}} = 1 + \frac{\Delta r_{ext}}{r_{ext,0}} = 1 + \frac{2r_{in,0}^2}{r_{ext,0}^2 - r_{in,0}^2}\frac{p_s}{E} \tag{14c}$$

The glossary of the symbols used is given in Table 1. This solution can be somewhat simplified when written in terms of the notation from engineering mechanics as [5]:

$$\Delta L = \frac{L_0}{E}\frac{r_i^2 p_s}{r_e^2 - r_i^2}(1-2\mu) \tag{15a}$$

$$\Delta r = \frac{r_i^2 p_s[r_e^2(1+\mu) + r^2(1-\mu)]}{rE(r_e^2 - r_i^2)} \tag{15b}$$

The systems of Eqs. (14) and (15) are equivalent.

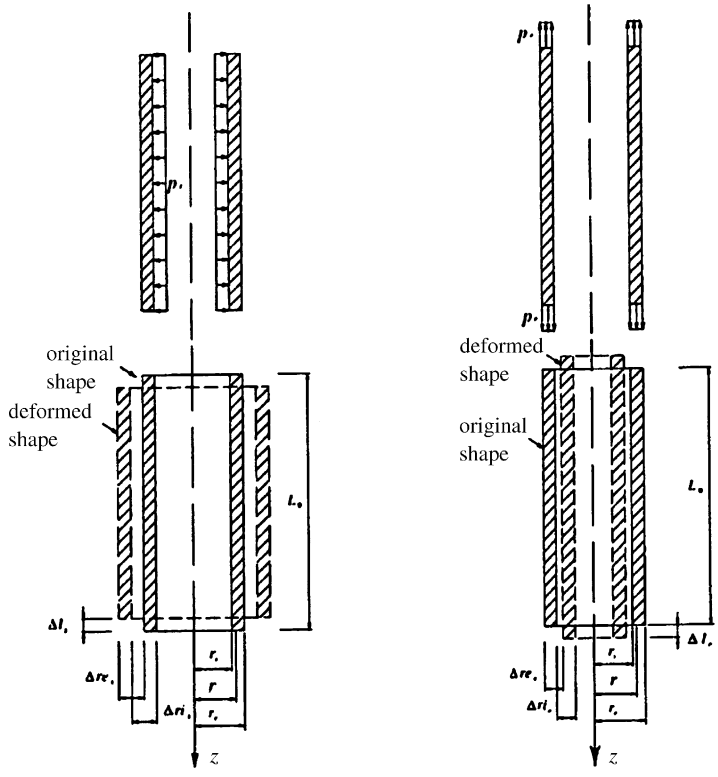

(a) Deformation caused by side pressure (b) Deformation caused by end pressure

Fig. 5. Superposition of radial and axial deformations in free end tube. Deformation caused by (a) side pressure and (b) end pressure.

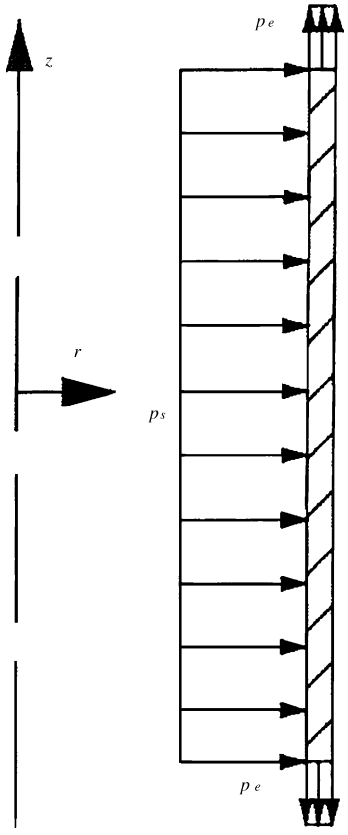

Fig. 6. Two-dimensional axis-symmetric model of the free end tube.

The analytical solution is based on a simplistic model for the tube, one for which the cylinder is of infinite length or the deformations are not affected by the end restraint. As shown in Fig. 1, an actual chromatography column is restrained by the end frits which tend to make the tube behave as if the ends of the tube are thicker than the tube. The actual end restraint depends on the stiffness of the cap and union system used in the HPLC instrument. An analytical solution does not exist for more realistic end conditions. However, numerical approximations such as the finite element method can be used to determine the deformation under such end conditions.

2.4. Finite element solution for radial and axial deformations

More realistic boundary or end conditions can be investigated using numerical approximations such as the finite element method. The degree of end restraint provided by the frits can be considered to be bound by two limit conditions:

(a) The free end case investigated above by the analytical solution, which provides the lower bound to the degree of rigidity of end restraint.
(b) The completely fixed end restraint, which provides an upper bound to the degree of rigidity of end restraint.

Actual chromatography tubes would have end conditions that lie somewhere between these two bounds, in most cases close to the second one due to the size and stiffness of the unions generally used to connect the column to the instrument. Fig. 7 illustrates schematically the free end, the fully retrained or very rigid end, and the intermediate end restraint conditions. Each of these end restraints can be investigated by the finite element method. The actual finite element model (Fig. 8) used an axis-symmetry mesh consisting of around 400 elements along one half of the 100 mm length, and two to four elements across the tube thickness, where the roller supports at sections A and B correspond to a line of symmetry at the midpoint of the tube.

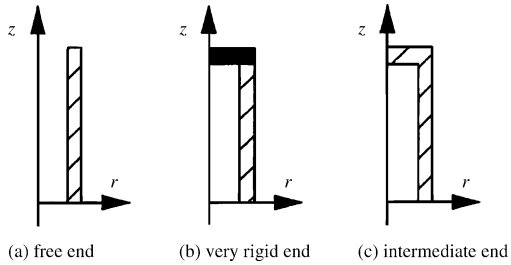

Fig. 7. Three conditions of end restraint (a) upper bound solution, (b) lower bound solution and (c) intermediate assumed condition.

2.4.1. Free column end (no end restraint)

A finite element model for the free end condition (Fig. 8; not to scale), was developed using the commercial finite element code ABAQUS 6.4 [9]. Because the end conditions are the same as in the analytical solution, the results should be comparable.

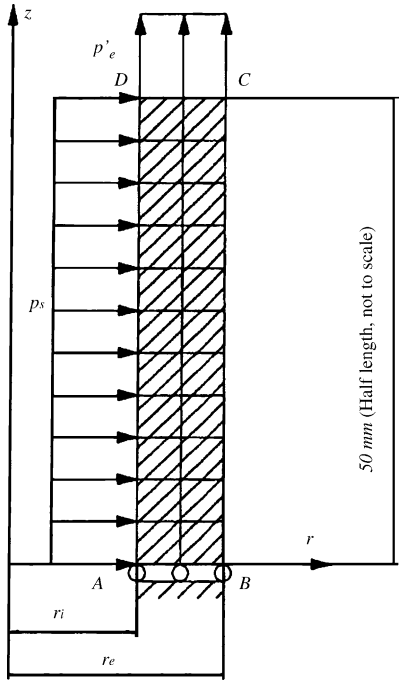

Fig. 8. Axis-symmetric finite element mesh for one-half the free end tube.

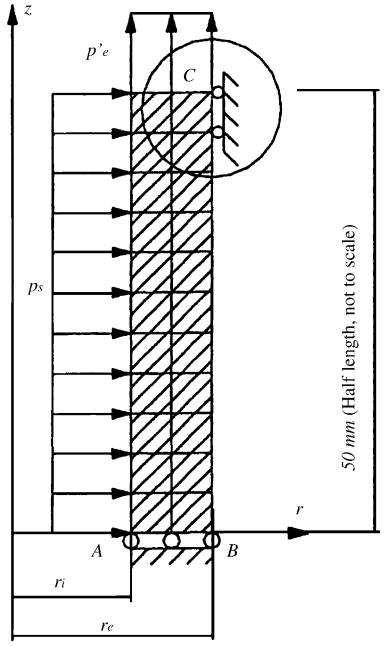

Fig. 9. Axis-symmetric finite element mesh for one-half the rigid-end tube.

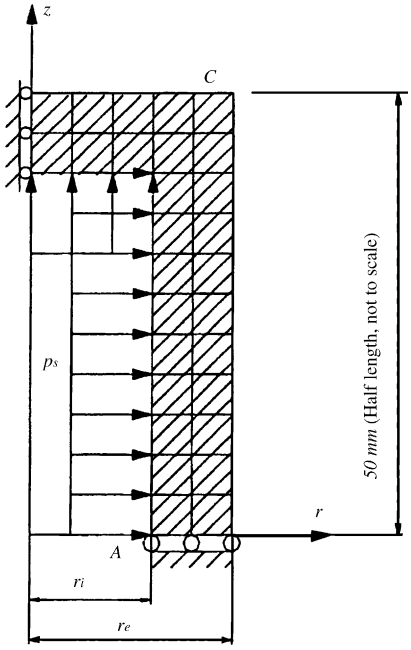

Fig. 10. Axis-symmetric finite element mesh for one-half the tube with a cap.

The axial stress in the tube is the same as in the analytical solution and

$$p'_{\mathrm{e}} = \frac{r_{\mathrm{i}}^2}{r_{\mathrm{e}}^2 - r_{\mathrm{i}}^2} p_{\mathrm{s}} \tag{16}$$

The analysis of the free end tube was also performed with a linear variation of radial pressure, corresponding to the actual condition in a chromatographic tube in which the mobile phase flows at a constant flow rate and a pressure gradient takes place across the length of the tube. An analytical solution for this loading case does not exist, but the numerical solution can be easily obtained by changing the uniform internal pressure, p_{s}, Fig. 8, to a linearly varying pressure with a maximum value of p_{s} and a minimum value of 0. Because the loading is no longer symmetrical, the entire length of the tube should be modeled.

2.4.2. Rigid column end—(complete end restraint)

In the case of the complete end restraint, it is assumed that the rigidity of the end plug is much larger than that of the tube itself, and that no relative displacement takes place between the tube end and the plug. Thus, the end of the tube is fixed in the radial direction, such that there is no radius change and no rotation angle in the tube end but that the tube remains free to expand in the *z*-direction (the end unions connect the column to fine connecting tubes which can accommodate freely any axial deformation of the column). There is no analytical solution available in this case but the finite element can easily be carried out, using a quarter axis-symmetrical, two-dimensional model, Fig. 9.

2.4.3. Hindered column end (intermediate end restraint)

Here we assume that the tube end is connected to an end cap that is not rigid enough to be considered as completely un-deformable. Calculations were made in the (arbitrary but reasonable) case in which the stiffness of both the tube and the cap are equal ($K_{\mathrm{p}}/K_{\mathrm{t}} = 1$). This boundary condition is illustrated in Fig. 10.

2.4.4. Comments

Because tubes used to pack chromatographic columns are very long and thin, with a very large aspect ratio, (L/r_{e}, typically 20–100), the boundary conditions at the tube end do not affect much its deformation at the center of the tube. This result can be explained by a straightforward application of the principle of Saint-Venant. The system of forces at the end of the tube is a balanced one. It produces a local bending that dies out rapidly as the distance along the *z*-axis from the restrained end increases [5].

Even though the analytical solution for a tube having free end (see analytical Eqs. (14a)–(14c) or (15a) and (15b)) neglects the rigidity of the column end, it can be used with sufficient accuracy to predict the deformation of chromatography tubes. It will be shown that it gives results that match well with those of the numerical solution obtained via finite element analysis, except in the regions close to the end restraint.

3. Results and discussion

In the cases investigated here, it was assumed that the internal pressure *P* was uniform along the length of the tube

Table 5
Stress components at the inner radius of typical chromatography tubes

Tube	Principal stresses (MPa)			Stress of interest (MPa)		
	σ_1	σ_2	σ_3	Rankine ($\sigma_{\theta\,\max}$)	Tresca ($\tau_{\max}$)	von Mises (σ_s)
SS-1	166.7	33.3	−100.0	166.7	133.3	33.3
SS-2	328.4	114.2	−100.0	328.4	214.2	114.2
SS-3	158.7	29.3	−100.0	158.7	129.3	29.3
SS-4	612.0	256.0	−100.0	612.0	356.0	256.0
SC-1	456.3	3.1	−450.0	456.3	453.1	3.1
SC-2	793.7	56.9	−680.0	793.7	736.9	56.9

Table 6
Calculated maximum internal pressure and factor of safety for typical tubes according to different theories of failure

Tube	Maximum internal pressure (MPa)			Factor of safety		
	$p_{s\_Rankine}$	p_{s_Tresca}	$p_{s\_Von\ Mises}$	$FS_{Rankine}$ (4)*	FS_{Tresca} (3)*	$FS_{Von\ Mises}$ (1.5)*
SS-1	565	353	1630	5.65	3.53	16.30
SS-2	287	220	476	2.87	2.20	4.76
SS-3	594	364	1850	5.94	3.64	18.50
SS-4	154	132	212	1.54	1.32	2.12
SC-1	4760	2400	398000	10.60	5.32	885.00
SC-2	4130	2230	33300	6.08	3.27	49.00

* Recommended value from [7].

to facilitate the solution. In practice, the energy loss across the tube length results in linear pressure gradient from P_{max} (which is in the kbar range) at the column inlet to 0 at the outlet. The numerical analysis was repeated to investigate the effect of the pressure gradient with a pressure of $p_s = P_{max}$ at the column inlet and a pressure of 0 at the outlet. The results indicate that the maximum radial deformation, Δr, which occurs at the middle portion of the column, and length change of the tube, ΔL, are both smaller in the case of the linearly varying pressure than with the uniform pressure. Thus, the uniform pressure distribution results in an overestimation (or conservative estimation) of the tube deformations. However, the effect of the linearly varying pressure may be more significant in an analysis of the stresses in the region near the connection between the column end and the frit, but this analysis requires details of the frit and geometry of the connection and is beyond the scope of this paper.

Thus, the comparative analysis of the stresses and deformations in chromatographic tubes with both a uniform pressure and a linear pressure gradient across the column shows that the uniform pressure is the worst case, Accordingly, this case will be considered for the remainder of the paper.

Table 7
Relative radius and length change of the chromatography tube (analytical, free end case)

Tube	Deformation			Strain		
	Δr_i (mm)	Δr_e (mm)	ΔL (mm)	$\Delta r_i/r_i$	$\Delta r_e/r_e$	$\Delta L/L$
SS-1	0.000472	0.000278	0.005567	0.000944	0.000278	0.000056
SS-2	0.003722	0.002998	0.019070	0.001618	0.000952	0.000191
SS-3	0.000455	0.000257	0.004897	0.000911	0.000244	0.000049
SS-4	0.007540	0.006775	0.042753	0.002800	0.002134	0.000428
SC-1	0.000109	0.000014	0.014226	0.007291	0.000079	0.000028
SC-2	0.000616	0.000257	0.257021	0.012324	0.001425	0.000514

Table 8
Computed deformation at points A– C (Fig. 8) from analytical and FE solutions of the free end tube

Tube	Internal radius change, point A (mm)		External radius change, point B (mm)		Length change, point C (mm)	
	Analytical	FEM	Analytical	FEM	Analytical	FEM
SS-1	4.72167×10^{-4}	4.72167×10^{-4}	2.77833×10^{-4}	2.77833×10^{-4}	5.56667×10^{-3}	5.56667×10^{-3}
SS-2	3.72209×10^{-3}	3.72209×10^{-3}	2.99817×10^{-3}	2.99817×10^{-3}	1.90703×10^{-2}	1.90703×10^{-2}
SS-3	4.55464×10^{-4}	4.55464×10^{-4}	2.56649×10^{-4}	2.56649×10^{-4}	4.89736×10^{-3}	4.89736×10^{-3}
SS-4	7.53950×10^{-3}	7.53950×10^{-3}	6.77478×10^{-3}	6.77478×10^{-3}	4.27526×10^{-2}	4.27526×10^{-2}
SC-1	1.09368×10^{-4}	1.09368×10^{-4}	1.41996×10^{-5}	1.41996×10^{-5}	1.42255×10^{-2}	1.42255×10^{-2}
SC-2	6.16196×10^{-4}	6.16196×10^{-4}	2.56554×10^{-4}	2.56554×10^{-4}	2.57021×10^{-1}	2.57021×10^{-1}

3.1. Computed stresses in typical chromatographic columns

As indicated in Table 2, it is assumed that the stainless steel tubes are subjected to an internal pressure of around 100 MPa, while the silica tubes are subjected to internal pressures of 450 and 680 MPa. Table 5 presents the calculated principal stresses and stress components ($\sigma_{\theta\,\max}$), ($\tau_{\max}$) and (σ_z) inside each tube using Eq. (1), where positive stresses indicate tension. It is noteworthy that the maximum tensile stress in tube SS-4 has a value of $\sigma_\theta = 612.0$ MPa which is more than six times the internal pressure. This tube is the thinnest with $r_m/t = 6.1$ which is approaching the $r_m/t = 10$ for "thin" tubes. Tube SS-2 ($r_m/t = 3.2$) has a σ_θ more than three times the internal pressure.

3.2. Comparison of the maximum allowable internal pressure and the factor of safety according to different theories of failure

The designs of most structures are based on formulas that are known to be approximate and use materials whose mechanical properties cover a relative band, due to the uncertain reproducibility of the properties of the sample and their environmental behavior not being thoroughly known. The use of factors of safety is a trade-off means of establishing equal reliability and safety by assigning to a single parameter varying degrees of quality assurance. This is the basis upon which many codes and standards are based.

The ASME pressure vessel code has several factors of safety based on different theories of failure, but with comparable safety and reliability. It permits lowering the factor of safety as the degree of quality insurance is successively increased or more refined failure theories are adopted as in Table 4.

The stress components for each of the six chromatography tubes defined in Table 2 were calculated in Table 5, based on the three failure theories summarized in Table 4. For purpose of comparison, the factor of safety was defined as:

$$\mathrm{FS} = \frac{\text{maximum internal pressure at failure}}{\text{assumed service pressure}} \tag{17}$$

Table 6 reports for each of the six tubes considered, the computed maximum allowable internal pressure according to the three failure theories (Table 4). Also shown is the computed FS according to Eq. (16) for each of the failure theories. The yield stress for the materials was taken as in Table 3. For the silica tubes, the maximum pressures are based on the tensile strength of the silica. It can be seen that the Rankine and Tresca theories give similar results, while the von Mises theory provides much larger maximum internal pressures (or smaller factors of safety). Tubes SS-2 and SS-4, which have higher r_m/t ratios (thinner tubes), are operating at the lowest factor of safety.

Table 9
Comparison of deformation at points A–C between free end (Fig. 8), intermediate end (Fig. 9) and restricted end (Fig. 10), FE solution

Tube	Internal radius change, point A (mm)			External radius change, point B (mm)			Length change, point C (mm)		
	Free end	Intermediate end	Restricted end	Free end	Intermediate end	Restricted end	Free end	Intermediate end	Restricted end
SS-1	4.72167×10^{-4}	4.72165×10^{-4}	4.72167×10^{-4}	2.77833×10^{-4}	2.77832×10^{-4}	2.77832×10^{-4}	5.56667×10^{-3}	5.45154×10^{-3}	5.59264×10^{-3}
SS-2	3.72209×10^{-3}	3.72265×10^{-3}	3.72259×10^{-3}	2.99817×10^{-3}	2.99867×10^{-3}	3.00361×10^{-3}	1.90703×10^{-2}	1.64877×10^{-2}	2.10276×10^{-2}
SS-3	4.55464×10^{-4}	4.55463×10^{-4}	4.55460×10^{-4}	2.56650×10^{-4}	2.56649×10^{-4}	2.56641×10^{-4}	4.89736×10^{-3}	4.79530×10^{-3}	5.21146×10^{-3}
SS-4	7.53950×10^{-3}	7.53231×10^{-3}	7.53951×10^{-3}	6.77478×10^{-3}	6.76762×10^{-3}	6.77480×10^{-3}	4.27526×10^{-2}	4.07906×10^{-2}	4.51170×10^{-2}
SC-1	1.09368×10^{-4}	1.09368×10^{-4}	1.09368×10^{-4}	1.41996×10^{-5}	1.41996×10^{-5}	1.41996×10^{-5}	1.42255×10^{-2}	1.42266×10^{-2}	1.42895×10^{-2}
SC-2	6.16196×10^{-4}	6.16196×10^{-4}	6.16196×10^{-4}	2.56554×10^{-4}	2.56554×10^{-4}	2.56554×10^{-4}	2.57021×10^{-1}	2.57156×10^{-1}	2.58142×10^{-1}

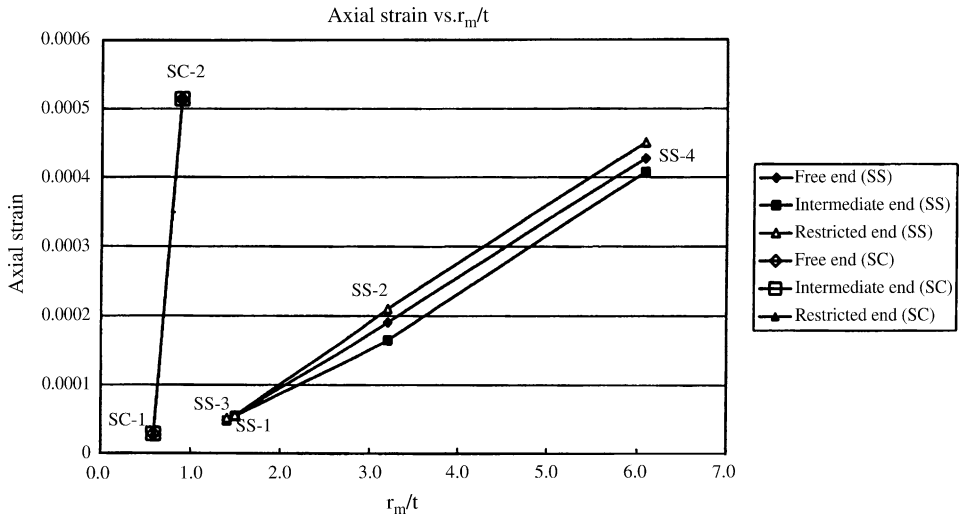

Fig. 11. Effect of r_m/t to axial strain of the tubes.

3.3. Computed dimensional change in typical chromography columns

Table 7 lists the computed radial and length change for each of the tubes from the analytical solution (free end condition). The maximum internal radial change does not exceed 0.01 mm (maximum value 0.0075 mm for SS-4) while the maximum length change occurs in SC-2 and is 0.257 mm due to the relative long length of this tube. The maximum relative internal radial strain ($\Delta r_i/r_i$) is 0.012324, the maximum relative external radial strain ($\Delta r_e/r_e$) is 0.001425, and the maximum relative axial strain ($\Delta L/L$) is 0.000514. It can be concluded that the changes in radius and length of the tubes are very small at points A, B, and C (Fig. 8).

Table 8 compares the radial and axial deformations for the free end conditions of the chromatographic columns evaluated with both the analytical and the finite element analysis. The results are in excellent agreement (the relative differences are less than 1×10^{-6}).

Table 9 compares the deformation at points A–C calculated for the boundary conditions with restricted, intermediate and free ends for the six tubes. The results show that the end restriction does not affect significantly either the deformation of the tube radius at the mid point of the column or its length change. Note, however, that the end restriction causes both a slight increase in the length expansion (about 5%) and a slight decrease in the radius change. Fig. 11 presents the relative axial strain ($\Delta L/L$) for different r_m/t ratio and Fig. 12 the relative internal ($\Delta r_i/r_i$) and external ($\Delta r_e/r_e$) radial strains for different r_m/t ratio of the four stainless steel and two silica tubes. As shown in these two figures, for the four stainless steel tubes (which have the same length), under equal internal pressure, both the axial and the radial strain increase with increasing r_m/t ratio. Combined with the zero change in the radii at both ends, these effects combine to keep constant the volume occupied by the metal. It can be concluded that the analytical solution, although it is approximate in the chromatographic tube case, can be

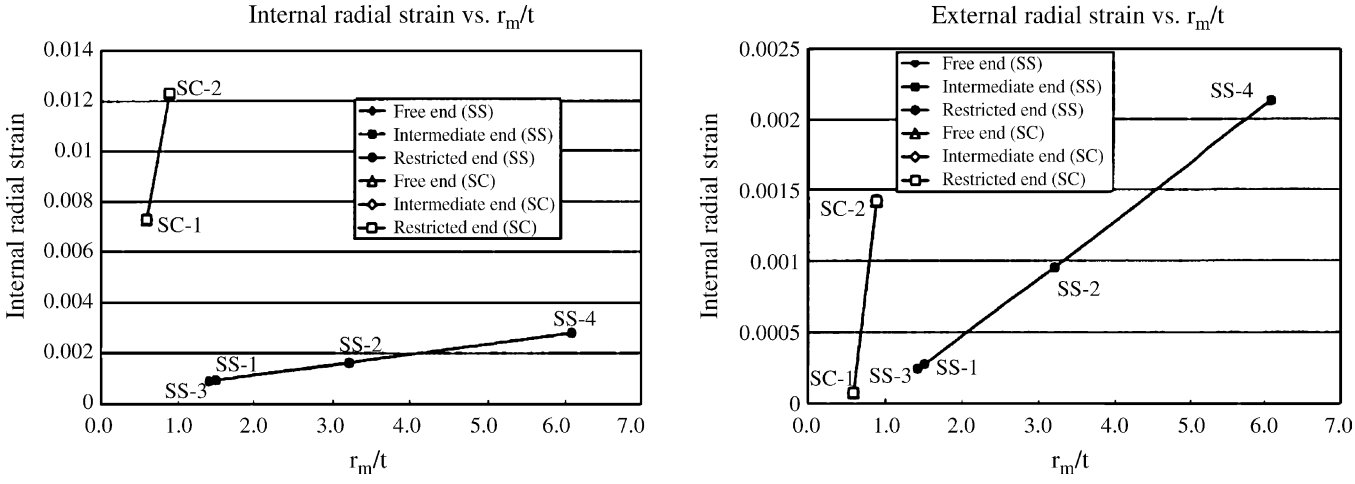

Fig. 12. Effect of r_m/t to internal and external radial strain of the tubes.

used to accurately predict the dimensional changes in these tubes.

Because the deformations and strains in all of the tubes are small, the energy stored in the deforaiation is also very small. The energy stored by compression of the liquid is also relatively small [1]. Thus, if a tube was to fail, The released strain energy would be moderate and of little consequence.

4. Conclusions

The stress components inside the wall of typical chromatographic column tubes were investigated through the principles of engineering mechanics, and the relevant stress quantities calculated for typical stainless steel and silica tubes. These stresses were compared with the yield stresses based on three well-known failure theories. The calculated stresses are expressed in terms of a safety factor, or ratio of the maximum internal pressure to service pressure. Based on the typical tube dimensions and operating pressures identified here, both the stainless steel and the silica tubes are safe when the von Mises failure theory is assumed. When the less rigorous Rankine and Tresca failure theories are used, the desired levels of safety are not achieved with the selected operating pressures above which failure would be expected.

An existing analytical solution for the deformations of chromatographic tubes was reviewed and presented in a simplified form. Numerical approximations by the finite element method are shown to agree with the analytical solution. This numerical solution was then used to explore the effect of various levels of end restraint. It is suggested that because most chromatographic tubes are very long with respect to their diameter, the effects of end restraint are very localized, and the expressions for free end tubes are appropriate. It is also shown that the deformations in typical chromatography columns under the assumed operating pressures are small.

References

[1] M. Martin, G. Guiochon, J. Chromatogr., in press.
[2] F. Gritti, M. Martin, G. Guiochon, J. Chromatogr. A 1070 (2005) 13.
[3] J.S. Mellors, J.W. Jorgenson, Anal. Chem. 76 (2004) 5441.
[4] Y. Shen, R. Zhang, R.J. Moore, J. Kim, T.O. Metz, K.K. Hixson, R. Zhao, E.A. Livesay, H.R. Udseth, R.D. Smith, Anal. Chem., 77, in press.
[5] S.P. Timoshenko, J.N. Goodier, Theory of Elasticity, McGraw-Hill, New York, NY, 1970.
[6] D.R. Moss, Pressure Vessel Design Manual: Illustrated Procedures for Solving Major Pressure Vessel Design Problems, Elsevier/Gulf Professional Publication, Amsterdam Boston, 2004.
[7] D.M. Fryer, J.F. Harvey, High Pressure Vessels, Chapman & Hall: International Thomson Publication/Thomson Science, New York, 1998.
[8] R.V. Juvinall, Engineering Considerations of Stress, Strain and Strength, McGraw-Hill, New York, 1967.
[9] ABAQUS 6.4 Habbitt, Karlsson and Sorensen Inc., Rhode Island, 2004.
[10] Polymicro Technologies, Mechanical Stress and Fiber Strength, http://www.polymicro.com/catalog/2_25.htm, 2004.
[11] Polymicro Technologies, Thick Wall Flexible Fused Silica Capillary Tubing, TSP: Standard Polyimide Coating, http://www.polymicro.com/products/capillarytubing/products_capillarytubing_tsp.htm, 2004.